Surface-sensitive Fe 2p photoemission spectra for α-Fe_2O_3(0001): The influence of symmetry and crystal-field strength

T. Droubay and S. A. Chambers
Environmental Molecular Sciences Laboratory, Pacific Northwest National Laboratory, Richland, Washington 99352
(Received 28 February 2001; published 2 November 2001)

We have measured high-energy-resolution Fe 2p photoelectron spectra for α-Fe_2O_3/α-Al_2O_3(0001) grown by oxygen-plasma-assisted molecular-beam epitaxy at emission angles chosen to enhance bulk and surface contributions. We quantitatively reproduce the subtle line-shape differences in these spectra by taking into account the break in symmetry and change in crystal field splitting generated by the presence of the surface.

DOI: 10.1103/PhysRevB.64.205414 PACS number(s): 75.50.Ee, 79.60.Bm, 81.15.Hi

I. INTRODUCTION

Metal core-level spectra of transition-metal compounds are enormously complex. They are affected by multiplet splitting, shake-up phenomena and the attendant satellite features, phonon broadening, and, in some cases, the presence of multiple oxidation states. The vast majority of all previous experimental photoemission investigations of transition-metal oxides utilized conventional nonmonochromatic x-ray sources, resulting in spectra with at best marginal energy resolution. As a result, the fine structure that exists in these spectra could not be resolved. In addition, most previous studies were not carried out under experimental conditions that yield truly surface sensitive spectra. One must obtain spectra at a photon energy that minimizes the photoelectron attenuation length, or at an emission angle sufficiently close to grazing to limit the spectral sensitivity to the top few atomic layers. One exception is a recent work by Nesbitt *et al.*[1] These authors used synchrotron radiation photoemission at high-energy resolution, and high surface sensitivity, to measure core-level spectra for cleaved pyrite. They then interpreted the spectra in light of surface electronic structure.

Several theoretical models have been proposed to interpret these complex photoemission line shapes and satellite structures in terms of the valence electron configurations.[2–5] Many of these methods involve the mixing of configurations arising from charge transfer from the ligand to the transition-metal ion. Zaanen *et al.*[4] calculated the Ni 2p core-level spectra utilizing the Anderson impurity framework for Ni dihalides and found a large variation in Ni-ligand charge-transfer energy. Okada *et al.*[6] expanded this model to include multiplet, spin-orbit, and crystal field splitting for Ni and Co dihalides. More recently, Bagus *et al.*[7] have challenged the traditional charge-transfer assignments and argued that all features in the photoemission spectra of MnO(001) can be accounted for with many electron atomic multiplet coupling and recoupling of the d-shell electrons. Fujii *et al.*[8] have carried out configuration interaction (CI) calculations to interpret core-level and valence-band photoemission measurements for iron oxide films grown by NO_2-assisted molecular beam epitaxy (MBE). Their theoretical method produced reasonably good agreement with experiment. However, this study, as most of the previous investigations, utilized nonmonochromatic Al$K\alpha$ x-rays, resulting in marginal energy resolution, and a spectrometer geometry that did not maximize surface sensitivity. As a result, spectral information specific to the first few atomic layers could not be obtained.

In order to more definitively learn how the presence of the surface affects these complex spectra, we have exploited differences in the Fe 2p photoemission line shape for α-Fe_2O_3(0001), as measured with state-of-the-art high-energy resolution x-ray photoemission spectroscopy (XPS) at normal, or bulk sensitive, and grazing, or surface sensitive, photoemission geometries. We can account for these differences by means of a relatively simple atomic multiplet theory, guided by Fe L-edge x-ray-absorption spectra (XAS) for α-Fe_2O_3. Values of the crystal field splitting in the bulk and at the surface are a result.

II. EXPERIMENT

Epitaxial α-Fe_2O_3 films were grown by oxygen-plasma-assisted molecular beam epitaxy (OPA-MBE) (Ref. 9) on α-Al_2O_3(0001) and then transferred under UHV conditions to an appended photoelectron spectroscopy chamber. Undoped, nonconductive films of thickness equal to ~2000 Å were grown at a substrate temperature of 400 °C and an initial growth rate of ~1 Å/min for the XPS experiments. After one hour the growth rate was increased to 0.1 Å s for the remainder of the film. Detailed accounts of the growth conditions are made elsewhere.[10] Following growth, x-ray photoelectron spectroscopy measurements were carried out in a connected chamber housing a GammaData SES-200 hemispherical analyzer with a monochromatic Al$K\alpha$ x-ray source and a precision goniometer/manipulator. Low-energy electron diffraction (LEED) patterns were also recorded in the photoemission chamber to further check crystallinity and cleanliness. An electron flood gun was used to compensate sample charging. All binding energies were referenced to that of O 1s, which was taken to be 530.0 eV.[10]

The x-ray absorption measurements were performed on the High-Energy-Resolution Monochromator (HERMON) beamline at the University of Wisconsin Synchrotron Radiation Center. With two interchangeable spherical gratings, HERMON operates over an energy range of 245–1100 eV with a flux of $\sim 10^{10}$photons/sec and is capable of delivering circularly polarized light throughout the energy range. X-ray absorption near-edge spectra were obtained from Fe_2O_3 powder pressed into indium foil, cut and polished naturally occurring hematite, and OPA-MBE α-Fe_2O_3 films grown on α-Al_2O_3(0001). XAS from these three specimens do not

show any appreciable line-shape differences. Division of the raw XAS spectra by the electron yield signal from a reference grid monitor measured concurrently with the sample was used for normalization. For fitting to theoretical data, we subtract a background intensity $I_B(E)$, which is calculated as

$$I_B(E) = \frac{1}{N} \int_{E_{\mathrm{MIN}}}^{E} I_M(e)de,$$

where the normalization factor N is defined so that the background equals unity above the edge, $I_B(E_{\mathrm{MAX}}) = 1$, which is the convention used for displaying the experimental data $I_M(e)$. The integration endpoints, $E_{\mathrm{MIN}} = 700$ eV and $E_{\mathrm{MAX}} = 735$ eV are chosen to be well below and above the edge. This background has the advantage that it is directly computed from the experimental data, and therefore requires no assumptions to be made about the shape of the background intensity.

III. CALCULATION METHOD

In order to interpret the Fe $2p$ XPS line shape in α-$Fe_2O_3(0001)$, we first consider the Fe L-edge XAS for α-Fe_2O_3 powder. There are two reasons for this approach. First, L-edge XAS spectra of first-row transition elements are characterized by very sharp multiplet features, limited by a core-level broadening of less than ~0.2 eV. These spectra are thus better resolved than their XPS counterparts, making their deconvolution easier. Second, there are no shake-up satellites present in XAS, thus simplifying their interpretation *vis à vis* XPS. However, it must first be established that it is legitimate to interpret XPS in light of XAS. In, XPS, the x-ray photon is of sufficient energy to excite the photoelectron to a final-state energy that is well above threshold. In contrast, the photon energy in XAS is at the threshold for excitation from the core orbital to the lowest unoccupied bound state. However, despite this difference, the final-state multiplets occur at the same relative energies in the two spectroscopies, as seen in Fig. 1. The reason for this result is that to first approximation, the Fe(III) ion is left in the same final state in the two experiments. The Fe(III) L-edge XAS transition in α-Fe_2O_3 can be described as $2p^6 3d^5 \rightarrow 2p^5 3d^6$. Virtually all workers in the field agree that the primary Fe $2p_{3/2}$ and $2p_{1/2}$ photoemission peaks (i.e., the ''nonsatellite'' peaks) originate from ligand-to-metal valence charge transfer accompanying Fe $2p$ core-hole creation, thereby leaving the Fe(III) ion in a $2p^5 3d^6 \underline{L}$ final state as the dominant configuration ($\underline{L}$ denotes an O $2p$ ligand hole). However, this unit of transferred charge is distributed among the six nearest-neighbor oxygen ligands, thereby amounting to only $\frac{1}{6}$ e^- transfer per ligand. If such a modification in charge distribution has a measurable effect on the magnitude of the crystal field, the multiplet energies in the Fe $2p$ core-level spectrum should be altered relative to those in the XAS. However, such is not the case, as Fig. 1 illustrates; the XPS and XAS multiplet energies are the same within our experimental resolution. Thus theoretical predictions of the more simple XAS multiplet structure can be used as a starting point to simulate the more complex and less well resolved XPS line shape.

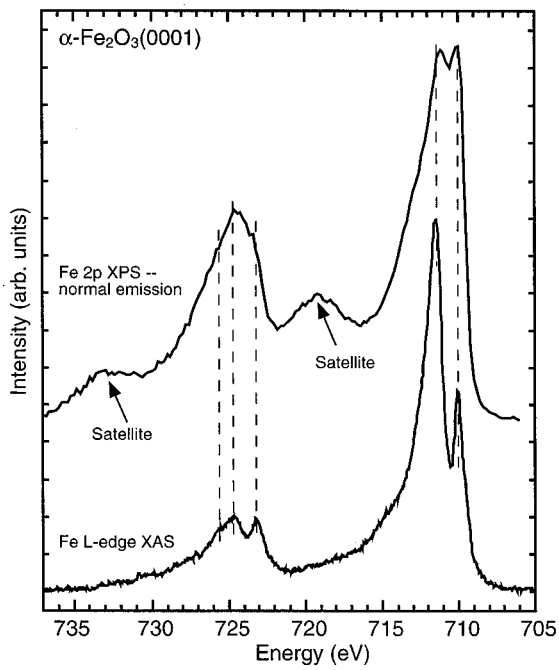

FIG. 1. Comparison of Fe L-edge XAS from hematite powder (bottom) with normal emission ($\theta = 90°$) Fe $2p$ XPS from α-$Fe_2O_3(0001)$ (top) with dashed lines to highlight similarities between $2p^5 3d^6$ and $2p^5 3d^6 \underline{L}$ final-state multiplet energies.

There has been considerable theoretical effort devoted to calculating x-ray absorption spectra with a range of methods including atomic models, a linear combination of atomic orbitals (LCAO) band-structure approach, and density-functional theory. Our approach is to use the ligand field multiplet model which has been described extensively earlier.[11] This simple atomic model is important for those experiments which are sensitive to symmetry and thus those experiments which involve only the $3d$ band. We consider the crystal field surrounding the metal ion from the point of view of symmetry reduction. The d orbitals, which are degenerate in spherical symmetry, split into two subsets of t_{2g} and e_g orbitals in an octahedral (O_h) crystal field. There is a break in degeneracy of the order of ~0.1 eV within the t_{2g} and e_g orbital sets associated with going from a purely octahedral field to the distorted octahedral field found in the corundum structure.[12] However, one can still fit the spectra using one parameter, $10Dq$, which is the energy difference between the centers of gravity of the t_{2g} and e_g orbital sets. For the surface-sensitive spectra, we consider a further reduction in symmetry to C_{3V} with the associated inversion of the t_{2g} and e_g orbital energies, as well as the attendant loss of degeneracy within each orbital subset. Here, the reported crystal field splitting is again the energy splitting between the geometric centers of the t_{2g} and e_g orbital sets. The Slater integrals were scaled to 80% of the associated atomic values, and $10Dq$ was varied from 0.8 to 2.4 eV as an optimal fit to experiment was sought. To obtain the theoretical spectrum from the discrete multiplets, the latter were broadened with a Lorentzian to simulate lifetime effects, and a Gaussian to simulate instrumental resolution. Lorentzian full width at

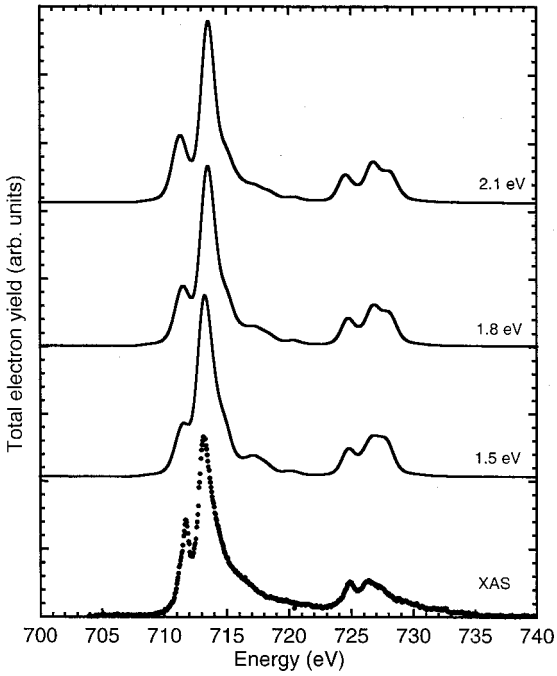

FIG. 2. Fe L-edge XAS of α-Fe_2O_3 (dotted line) compared with a ligand field multiplet calculation with crystal field strength 2.1, 1.8, and 1.5 eV (solid line) from top to bottom.

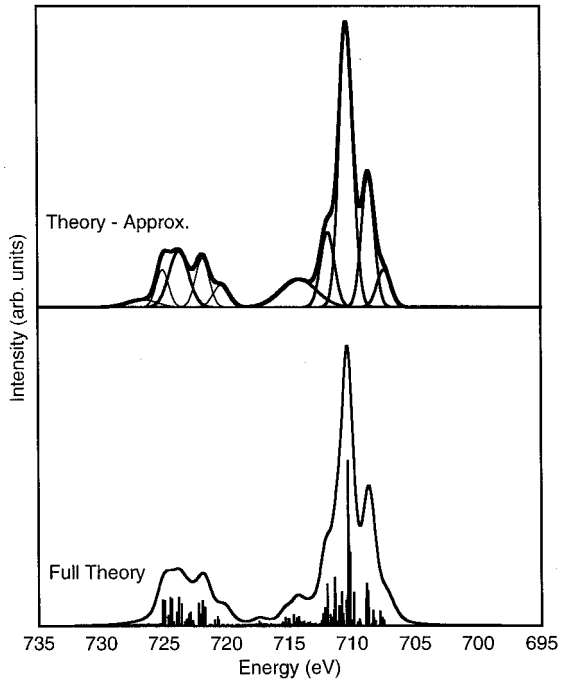

FIG. 3. Discrete multiplets (sticks) and convolution (bottom) for Fe(III) in octahedral symmetry and an approximation (top) composed of ten broadened representative multiplets. The crystal field strength corresponds to $10Dq = 1.8$ eV.

half maximum (FWHM) values of 0.30 and 0.10 eV were used for multiplets in the L_2 and L_3 peak manifolds, respectively, whereas a 0.3 eV Gaussian FWHM was used for all multiplets. The broadening used for multiplets in the L_3 manifold differed from that used in the L_2 manifold to account for the extra decay channel present in the latter.[13]

Figure 2 shows the experimental Fe L-edge XAS from α-Fe_2O_3 (bottom), along with atomic multiplet calculations for Fe(III) in a purely octahedral symmetry for three values of the crystal field splitting—1.5, 1.8, and 2.1 eV—using the broadening scheme discussed above. While examination of the experimental XAS at the L_3 manifold clearly reveals better resolution for transitions at lower photon energy, representative values of the lifetime broadenings for each spin-orbit manifold and the overall experimental broadening were used to reproduce the whole of the line shape. However, enhanced resolution at lower photon energies suggests that the lifetimes may vary systematically with energy. The best fit between experiment and the full ligand field multiplet calculation occurs for a crystal field splitting ($10Dq$) of 1.8 eV, as determined by the chi-squared value for a range of values between $10Dq = 0$ and 3.0 eV. A similar treatment was done by van der Laan and Kirkman whom also report a best fit for crystal field value of 1.8 eV.[14] Here, chi-squared was defined as

$$\chi^2 = \frac{\Sigma (I_M - I_T)^2}{\Sigma I_M},$$

where I_M and I_T are the background-subtracted experimental XAS and the calculated intensities, respectively.

Rather than using the entire set of multiplets, which exceeds 100, ten representative Gaussian/Lorentzian broadened multiplet peaks were chosen to represent the atomic multiplet calculation. These peaks were chosen because their binding energies were common to those of large numbers of closely spaced and unresolvable multiplets. This set of ten is thus representative of the total multiplet set. We show in Fig. 3 the total multiplet set (sticks) along with the total theoretical spectrum (bottom) obtained by convolution of the individual multiplets with the Lorentzian and Gaussian curves discussed above. The upper panel of Fig. 3 shows the set of ten representative Gaussian peaks whose individual height and full width at half maximum (FWHM) were varied in order to achieve the best fit, along with their sum. The sum of the ten representative multiplets (top) compares very favorably with both the theoretical (bottom) and experimental spectrum (Fig. 2). Independent determination of the ten representative curves that best simulate the total calculation was repeated for each value of $10Dq$.

IV. PHOTOEMISSION RESULTS AND DISCUSSION

We show in Fig. 4 high-energy resolution Fe 2p core-level spectra for α-Fe_2O_3(0001) taken at normal emission, $\theta = 90°$ (top), and at grazing emission, $\theta = 7°$ (bottom), relative to the surface. All major features (A–E), are present at both emission angles. However, there is a shift to higher binding energy for peak A with respect to the remaining peaks (B–E) at grazing emission. Peaks C and E are the satellite features associated with the $2p_{3/2}$ and $2p_{1/2}$ peaks, respectively, and originate from the $2p^5 3d^5$ final state of the Fe(III) ion in which there is no charge transfer from the

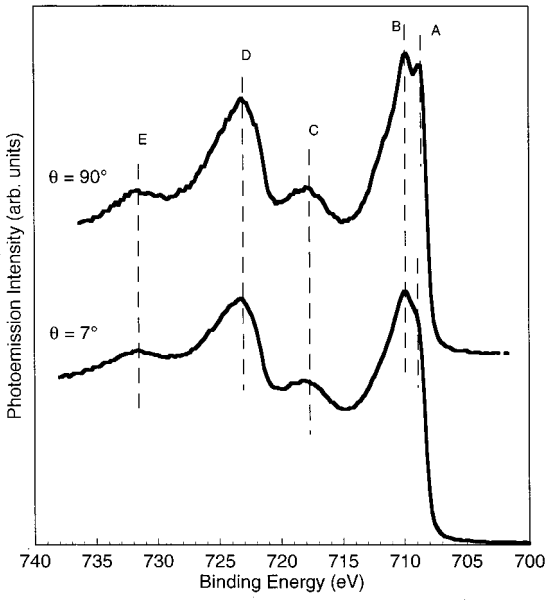

FIG. 4. High-energy-resolution Fe $2p$ core-level spectra for α-$Fe_2O_3(0001)$ obtained at normal emission ($\theta=90°$), top, and grazing emission angle ($\theta=7°$), bottom.

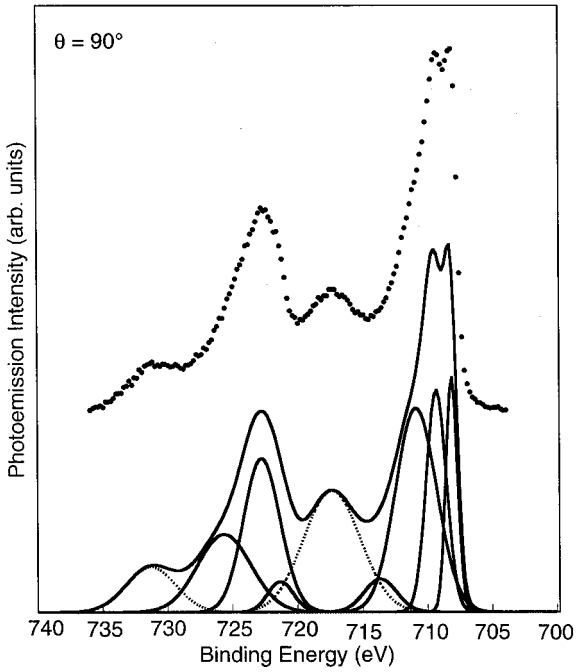

FIG. 5. Measured XPS spectrum for α-$Fe_2O_3(0001)$ (dots) obtained at normal emission ($\theta=90°$), along with the simulated spectrum (solid curve) using the ten representative peaks from the XAS peak fit shown in Fig. 3 as a starting point.

ligand. The small yet distinct differences in the two spectra, especially visible in the $2p_{3/2}$ primary peak, are due to differences in geometric and electronic structure at the surface relative to the bulk. Fe atoms in the terminal layer sit in threefold hollow sites created by the underlying plane of oxygen atoms with an inward relaxation of 0.5 ± 0.1 Å.[15] These atoms thus possess C_{3V} symmetry instead of the nearly perfect octahedral symmetry of the bulk.

The reduced multiplet peak set found to accurately reproduce the Fe L-edge XAS was used to simulate the Fe $2p$ XPS spectrum at normal emission, with the addition of the two Gaussians to account for the satellites, which are not present in XAS and are not predicted by the simple theory. The XAS multiplet binding energies were not changed in simulating the Fe $2p$ core level at normal emission. The multiplet peak heights were allowed to vary in order to compensate for the different values of coupling between the core hole and the valence electrons in photoemission. The FWHM values were also allowed to vary to compensate for the additional experimental broadening in the photoemission spectra created by lifetime effects. Figure 5 compares the measured (dots, upper) and simulated (solid curve, lower) Fe $2p$ spectra at normal emission ($\theta=90°$). A standard Shirley background was subtracted from the experimental spectrum with the window taken to encompass the entire $2p_{3/2}$ and $2p_{1/2}$ region. The separation between the resolved multiplets in the $2p_{3/2}$ primary peak is very well reproduced, and reflects the goodness of the fit. The use of a common set of multiplets for XAS and normal-emission XPS, together with the excellence of the fits, validates the essential assumption that the $2p^53d^5$ and $2p^53d^6\underline{L}$ photoemission final states can indeed be treated separately. In addition, the physical similarity between the $2p^53d^6\underline{L}$ XPS and $2p^53d^6$ XAS final states is further validated, because theoretical predictions of both XPS and XAS reveal substantial sensitivity to $3d$ electron count. It is noteworthy that separate normal-emission Fe $2p$ simulations in which the crystal field strength was allowed to freely vary did not result in a more accurate simulation than that described above; a value of 1.8 ± 0.1 eV also resulted from this exercise.

We show in Fig. 6 a plot of chi squared as a function of

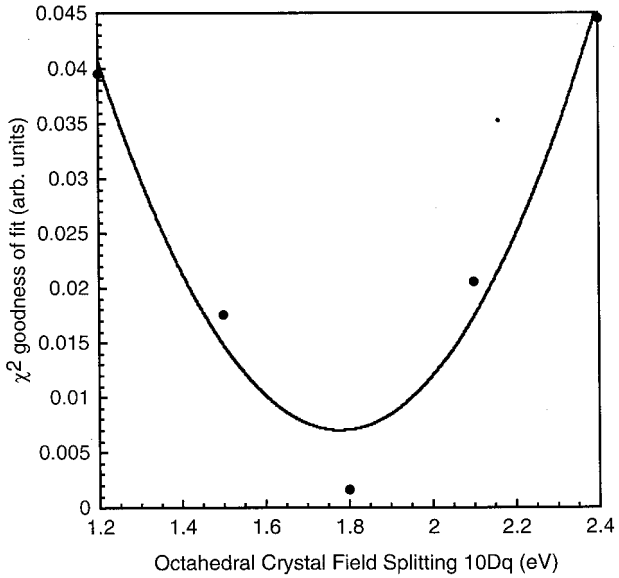

FIG. 6. χ^2 vs $10Dq$ for bulk-sensitive experimental Fe $2p$ XPS and simulated photoemission for Fe(III) ions in a purely octahedral field.

assumed crystal field splitting for the normal-emission Fe $2p$ spectrum. The optimal value for $10Dq$ for bulk α-Fe_2O_3, $1{:}8 \pm 0.1$ eV, obtained by the chi-squared analysis shown in Fig. 6, agrees fairly well with optical absorption measurements by Wickersheim and Lefever.[16] These authors report a value of 2.0 eV for natural α-Fe_2O_3. A somewhat different value is extracted from comparison of Fe_2O_3 XAS with CI calculations, which yielded a value of 1.5 eV.[17] It should be noted that the value of the crystal field strength yielded by our analysis contains only the electrostatic portion of the total crystal field parameter. The total parameter also contains a covalent contribution, which is not accounted for using our simple model.

Comparing spectra at normal and grazing emission angles allows the surface contribution to be differentiated from that of the bulk. Based upon a simple inelastic attenuation model with an electron attenuation length of $\sim$10 Å,[15] the probe depth at $\theta = 7°$ is approximately four atomic layers with $\sim$85% of the signal coming from the first two atomic layers. In contrast, the sampling depth at $\theta = 90°$ is approximately 30 layers, with 85% of the signal coming from the top $\sim$22 layers. The more surface-sensitive spectrum ($\theta = 7°$) differs from the more bulk sensitive spectrum primarily in the multiplet structure at the top of the $2p_{3/2}$ primary peak, which is less resolved in the spectrum obtained at $\theta = 7°$.

We followed much the same procedure to simulate the Fe $2p$ XPS obtained at grazing emission, except that $10Dq$ was allowed to vary, and the local symmetry of Fe(III) was changed to reflect the true surface structural environment.[15] The calculation was performed using C_{3V} symmetry, rather than the perfect octahedral (O_h) symmetry used for the normal emission simulation. We made this change in order to simulate the surface electronic structural environment as accurately as possible, although the effect is rather small, as discussed below. The same initial Lorentzian lifetime and Gaussian broadening were used, as previously determined by comparison to experimental XAS for the octahedral calculation. We show in Fig. 7 the important broadened multiplet peaks, their sum, and the experimental grazing-emission spectrum. The satellites shown as dashed curves were again represented by Gaussians, identical to the ones used for the bulk-sensitive simulation. The best agreement between theory and experiment occurs when a reduced value of 1.5 ± 0.1 eV was used for the crystal field splitting. Determination of the best fit was found by minimization of chi-squared as $10Dq$ was varied. The chi-squared curve shown in Fig. 8 can be represented by a parabola with minimum near 1.5 eV. A reduction in symmetry from O_h to C_{3V} alone will not account for the differences between the normal- and grazing-emission Fe $2p$ spectra. The changes produced by the reduction in symmetry were relatively small, whereas the dependence of the line shape on the crystal field is strong. This result is consistent with the experimental observation that deviations in ligand field symmetry produce only subtle lineshape changes in the Fe L-edge XAS of a number of Fe(III)-containing compounds.[16] Thus a reduction in the crystal field strength is required to account for the differences in line shapes.

We have investigated in detail the evolution of the surface morphology as a function of film thickness and growth conditions for the α-Fe_2O_3/α-$Al_2O_3(0001)$ system, and the results are relevant to our analysis of the surface-sensitive Fe $2p$ spectrum. A modified form of Stranski-Krastanov growth occurs as a result of the 5.8% lattice mismatch, resulting in

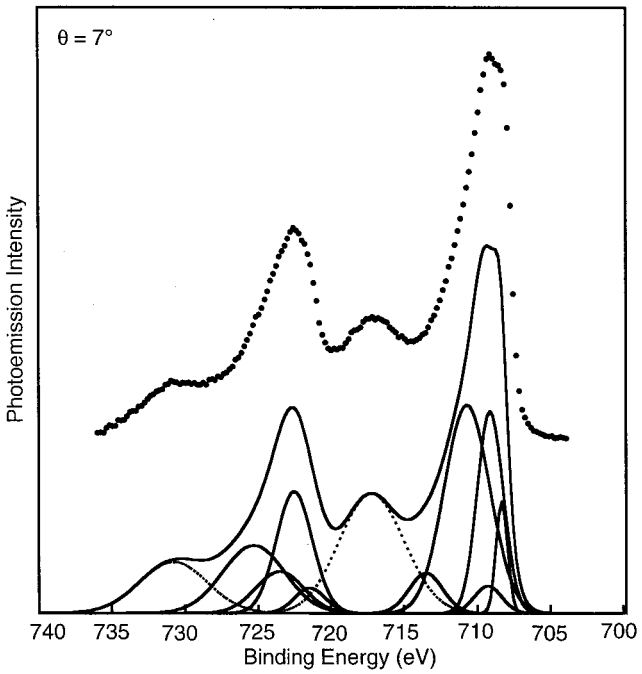

FIG. 7. Measured Fe $2p$ spectrum for α-$Fe_2O_3(0001)$ taken at grazing emission ($\theta = 7°$), top, along with the simulated spectrum (solid). The individual broadened multiplet curves are characteristic of local C_{3V} symmetry for Fe(III) at the surface, and $10Dq = 1.5 \pm 0.1$ eV.

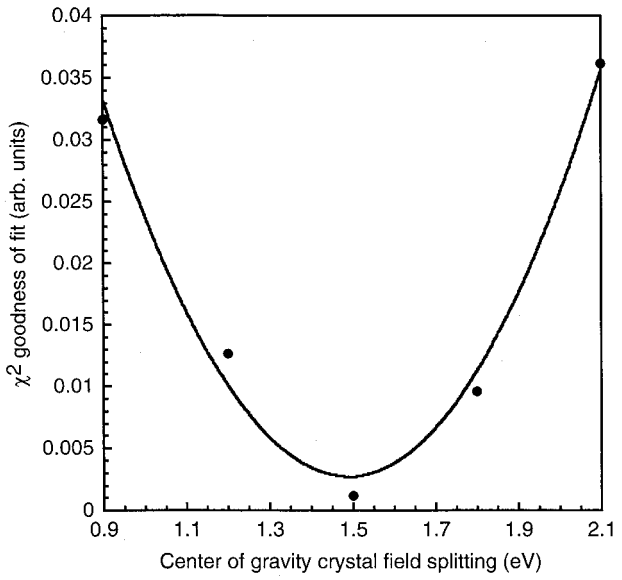

FIG. 8. χ^2 vs $10Dq$ for surface-sensitive experimental Fe $2p$ XPS ($\theta = 7°$) and simulated photoemission for Fe(III) ions in a C_{3V} field.

the formation of elongated islands along $[11\bar{2}0]$ at film thicknesses of a few tens of Å.[10,17] These islands coalesce with increasing film thickness, resulting in terraces that are several hundred Å in length along $[11\bar{2}0]$ at film thicknesses in excess of ~1000 Å. However, the step density along the orthogonal $[1\bar{1}00]$ direction remains high. The typical terrace width along this direction at ~2600 Å film thickness is ~20–25 Å, with 2.3 Å step heights between terraces of like Fe termination.[18] From this morphology, we estimate that ~20% of Fe cations in the surface layer are at steps and thus possess one or two dangling bonds per ion. Fe ions at steps are also of lower symmetry than either surface Fe ions on terraces, which exhibit C_{3V} symmetry, or bulk Fe ions, which possess distorted O_h symmetry. This morphological result is qualitatively consistent with the appearance of an OH-derived feature in the surface-sensitive O 1*s* spectra of these film surfaces, which exhibit intensities that are consistent with a partial monolayer of adsorbed OH.[15] Chemisorption studies on these OPA-MBE grown surfaces suggest that dissociative chemisorption of water occurs at steps below a threshold pressure of $\sim 10^{-4}$ torr, and that OH binds to Fe ions at these steps.[19] Chemisorption of OH was concluded to occur at Fe sites on terraces for pressures above the threshold pressure. The presence of Fe emitters at steps in the surface layer is expected to partially diminish the difference between bulk- and surface-sensitive Fe 2*p* spectra, because such ions have coordinations that are intermediate between Fe on the ''perfect'' surface and in the bulk. Nevertheless, an effect is clearly observed in the present experiment, and ~80% of surface Fe ions are estimated to be on terrace sites. Such ions possess C_{3V} symmetry and have three dangling bonds. In addition, the use of an oxygen plasma during growth and oxygen-rich conditions essentially preclude the formation of oxygen vacancies, which are expected to constitute the dominant class of point defects on this surface.

Our analysis of high-energy-resolution Fe 2*p* spectra for epitaxial γ-Fe_2O_3(001) (Ref. 20) yields the same conclusion regarding a reduction in crystal field strength from 1.8 to 1.5 eV at the surface. Spectra obtained at normal and grazing angle emission display a very subtle difference in the multiplet peak separation present in the primary $2p_{3/2}$ peak, which is only observable with high-energy resolution. As in the present case, these differences can be accounted for by modeling a reduction in crystal field strength at the surface.

V. CONCLUSIONS

In summary, we have demonstrated that Fe 2*p* spectral line shapes from α-Fe_2O_3(001), obtained in bulk- and surface-sensitive emission geometries at high-energy resolution, are sensitive to the break in symmetry and reduction in crystal field strength associated with the surface. With the aid of ligand field multiplet theory, which is highly sensitive to symmetry and crystal field parameters, in conjunction with x-ray-absorption spectroscopy, the core-level photoemission spectra can be deconvolved into individual final-state multiplets. With this approach, values of the crystal field splitting in the bulk (1.8 ± 0.1 eV) and at the surface (1.5 ± 0.1 eV) are obtained.

ACKNOWLEDGMENTS

The research described in this paper was performed in the Environmental Molecular Sciences Laboratory, a national scientific user facility sponsored by the Department of Energy's Office of Biological and Environmental Research and located at Pacific Northwest National Laboratory. This work was supported by the U.S. Department of Energy Environmental Management Science Program and the U.S. Department of Energy, Office of Science, Office of Basic Energy Sciences, Division of Materials Science.

[1] H. W. Nesbitt, M. Scaini, H. Hochst, G. M. Bancroft, A. G. Schaufuss, and R. Szargan, Am. Mineral. **85**, 850 (2000).
[2] S. Asada and S. Sugano, J. Phys. Soc. Jpn. **41**, 1291 (1976).
[3] J. Zaanen and G. A. Sawatsky, Phys. Rev. B **33**, 8074 (1986).
[4] J. Zaanen, C. Westra, and G. A. Sawatzky, Phys. Rev. B **33**, 8060 (1986).
[5] T. Uozumi, K. Okada, A. Kotani, R. Zimmermann, P. Steiner, S. Hufner, Y. Tezuka, and S. Shin, J. Electron Spectrosc. Relat. Phenom. **83**, 9 (1997).
[6] K. Okada, A. Kotani, and B. T. Thole, J. Electron Spectrosc. Relat. Phenom. **58**, 325 (1992).
[7] P. S. Bagus, R. Broer, W. A. d. Jong, W. C. Nieuwpoort, F. Parmigiani, and L. Sangaletti, Phys. Rev. Lett. **84**, 2259 (2000).
[8] T. Fujii, F. M. F. d. Groot, G. A. Sawatsky, F. C. Voogt, T. Hibma, and K. Okada, Phys. Rev. B **49**, 3195 (1999).
[9] S. A. Chambers, Surf. Sci. Rep. **39**, 105 (2000).
[10] S. I. Yi, Y. Liang, S. Thevuthasan, and S. A. Chambers, Surf. Sci. **443**, 212 (1999).
[11] F. M. F. deGroot, J. Electron Spectrosc. Relat. Phenom. **67**, 529 (1994).
[12] F. M. F. deGroot, Physica B **208/209**, 15 (1995).
[13] S. A. Chambers, S. Thevuthasan, Y. J. Kim, J. Morais, R. Denecke, C. S. Fadley, P. Liu, T. Kendelewicz, and G. E. Brown, Jr., Surf. Sci. **425**, 276 (1999).
[14] K. A. Wickersheim and R. A. Lefever, J. Chem. Phys. **36**, 844 (1960).
[15] S. Thevuthasan, Y. J. Kim, S. I. Yi, S. A. Chambers, J. Morais, R. Denecke, C. S. Fadley, P. Liu, T. Kendelewicz, and G. E. Brown, Jr., Surf. Sci. **425**, 276 (1999).
[16] T. Droubay, Ph.D. thesis, University of Wisconsin-Milwaukee, 1999.
[17] S. I. Yi, Y. Liang, and S. A. Chambers, J. Vac. Sci. Technol. A **17**, 1737 (1999).
[18] S. A. Chambers and S. I. Yi, Surf. Sci. Lett. **439**, L785 (1999).
[19] Ping Liu, T. Kendelewicz, G. E. Brown, Jr., E. J. Nelson, and S. A. Chambers, Surf. Sci. **417**, 53 (1998).
[20] S. A. Chambers and S. A. Joyce, Surf. Sci. **420**, 111 (1999).